

# Phenotypic Resistance in Photodynamic Inactivation Unravelled at the Single Bacterium Level

Sol R. Martínez,<sup>†</sup> Yohana B. Palacios,<sup>†</sup> Daniel A. Heredia,<sup>‡</sup> Maximiliano L. Agazzi,<sup>†</sup> and Andrés M. Durantini<sup>\*,‡,§</sup>

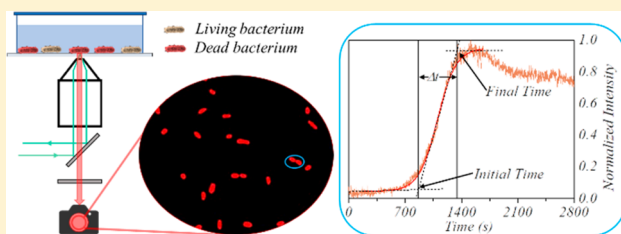
<sup>†</sup>Departamento de Química, Facultad de Ciencias Exactas, Físico-Químicas y Naturales, Universidad Nacional de Río Cuarto, Ruta Nacional 36 Km 601, X5804BYA Río Cuarto, Córdoba, Argentina

<sup>‡</sup>IDAS-CONICET, Departamento de Química, Facultad de Ciencias Exactas, Físico-Químicas y Naturales, Universidad Nacional de Río Cuarto, Ruta Nacional 36 Km 601, X5804BYA Río Cuarto, Córdoba, Argentina

## Supporting Information

**ABSTRACT:** Herein we report a simple fluorescence microscopy methodology that, jointly with four photosensitizers (PSs) and a cell viability marker, allows monitoring of phenotypic bacterial resistance to photodynamic inactivation (PDI) treatments. The PSs, composed of BODIPY dyes, were selected according to their ability to interact with the cell wall and the photoinactivating mechanism involved (type I or type II). In a first approach, the phenotypic heterogeneity allowing bacteria to persist during PDI treatment was evaluated in methicillin-resistant *Staphylococcus aureus* (MRSA) and *Escherichia coli* as Gram-positive and Gram-negative models, respectively. By means of propidium iodide (PI), we monitored with spatiotemporal resolution cell viability at the single bacterium level. All the PSs were effective at inactivating pathogens; however, the cationic nonhalogenated PS (compound 1) surpassed the others and was capable of photoinactivating *E. coli* even under optimal growth conditions. Compound 1 was further tested on two other Gram-negative strains, *Pseudomonas aeruginosa* and *Klebsiella pneumoniae*, with outstanding results. All bacterial strains used here are well-known ESKAPE pathogens, which are the leading cause of nosocomial infections worldwide. Thorough data analysis of individual cell survival times revealed clear phenotypic variation expressed in the cell wall that affected PI permeation and thus its intercalation with DNA. For the same bacterial sample, death times may vary from seconds to hours. In addition, the PI incorporation time is also a parameter governed by the phenotypic characteristics of the microbes. Finally, we demonstrate that the results gathered for the bacteria provide direct and unique experimental evidence that supports the time–kill curve profiles.

**KEYWORDS:** photodynamic inactivation, ESKAPE pathogens, photoactive molecules, phenotypic resistance, fluorescence microscopy, single cell



Antibiotics have revolutionized the world of science and medicine. Since 1940, antibiotics have been produced to eliminate pathogenic microorganisms. However, microbes have developed the ability to overcome these treatments with specific mutations on the targets, resulting in changes in bacterial susceptibility.<sup>1–4</sup> Statistics indicate that multidrug-resistant (MDR) bacteria, called “superbugs”, could cause more than 10 million deaths worldwide by the year 2050 and have an estimated global economic burden of US\$100 trillion.<sup>5</sup> In response to this latent threat, scientists have begun to develop alternative therapies, such as photodynamic inactivation (PDI), which emerged late in the 20th century as a promising treatment for killing pathogens. PDI requires the combination of light, a photosensitizer (PS), and molecular oxygen. Upon irradiation of the PS, the excited singlet state ( $S_1$ ) is populated and can undergo fast intersystem crossing (ISC) to a long-lived excited triplet state ( $T_1$ ). From  $T_1$ , electron transfer or energy transfer can occur, giving rise to what are known as type I and type II photoprocesses, respectively.<sup>6</sup> The former involves an electron transfer process

generating superoxide anion radicals ( $O_2^{\cdot-}$ ) that can be reduced to hydrogen peroxide ( $H_2O_2$ ) and subsequently induce the highly toxic hydroxyl radicals ( $OH^{\cdot}$ ) by Fenton chemistry. The type II mechanism uses energy transfer to generate singlet oxygen ( $^1O_2$ ).<sup>6–8</sup> In both cases, cytotoxic reactive oxygen species (ROS) are produced with the ability to oxidize lipid bilayers, DNA, proteins, and other biomolecules.<sup>9</sup>

ROS in cells can be formed by endogenous and exogenous sources.<sup>10,11</sup> Endogenous oxidants are produced as byproducts of aerobic metabolism. On the other hand, exogenous ROS refers to oxidants that are induced by extracellular factors such as ultraviolet light, chemotherapeutics, and environmental toxins, among others.<sup>10</sup> Nevertheless, ROS levels within certain boundaries are essential for maintaining cellular homeostasis, and many of them act as signaling molecules.<sup>12,13</sup> Regardless of

Received: May 18, 2019

Published: July 9, 2019

their origins, when these oxidants exceed safe limits, they became cytotoxic, affecting physiological functions.

Bacteria have different strategies to overcome the effects of drugs. The antibiotic response of a strain is classified as susceptible, tolerant, resistant, and persistent.<sup>14</sup> A bacterial culture is susceptible when the whole population is inhibited or killed by the presence of an antibiotic. The term resistant is associated with the failure of the antimicrobial therapy.<sup>15</sup> Unlike resistant microbes, persistence defines a genetically identical bacterial population in which a subpopulation (~2%) is not susceptible to the therapy.<sup>14,16–18</sup> This subpopulation can undergo transient and reversible changes in the bacterial phenotype that confer resistance to the antibiotic.<sup>14</sup> It has been demonstrated that the ability of persister cells to survive for longer periods is directly related to sporadic changes in gene expression, which modifies the properties of the cellular envelope.<sup>16</sup> Also, gene expression can affect the influx and efflux of solutes through membrane permeability, enabling bacteria to inhabit different and often hostile environments.<sup>19,20</sup> All of these factors are phenotypically expressed in each bacterium, revealing a particular composition of the cell wall.

The above definitions are solely for bacteria treated with antibiotics; however, there is no clear terminology in the PDI field. In this manuscript, we will be referring to the PDI treatment resistance of a bacterium within a subset of a genetically and metabolically identical bacterial population. Specifically, resistance in this work will point out the ability of microbes to endure different periods of treatment through phenotypic variations. It is our eagerness to demonstrate how bacterial survival times depend on the phenotype. We aim to visualize in real-time shorter and longer living individuals during a specific inactivation therapy.

To achieve our goal, we carefully selected four BODIPY-derivative PSs with different photodynamic mechanisms and specific binding groups, along with a well-known cell-death marker, propidium iodide (PI). PI is an effective indicator dye that becomes fluorescent upon intercalating with DNA.<sup>21</sup> Staining with red emitting PI depends directly on cell membrane permeability and is commonly used to evaluate cell viability.<sup>22,23</sup> As a proof of concept, we studied the following bacterial strains: methicillin-resistant *Staphylococcus aureus* (MRSA) as a Gram-positive model and *Escherichia coli*, *Pseudomonas aeruginosa*, and *Klebsiella pneumoniae* as Gram-negative models. These four strains are members of the well-known ESKAPE pathogens, which are the leading cause of nosocomial infections throughout the world.<sup>24</sup>

The simple experimental methodology described herein allowed us to monitor heterogeneity at the spatiotemporal level in the survival times of individual cells. This consequence is mainly due to phenotypic variations expressed in the cell wall, resulting in increased or reduced resistance toward photo-oxidation.

## RESULTS AND DISCUSSION

**Selection and Design of the PSs.** To pursue our goal, we choose four BODIPY-derivative photosensitizers. These compounds are shown in Figure 1, and each of them has a distinct characteristic. Compound 1, identified by a relatively low fluorescence quantum yield ( $\Phi_f$ ) compared with those of the other nonhalogenated BODIPY analogues and a negligible singlet oxygen quantum yield ( $\Phi_\Delta$ ) has proven to be an effective ROS generator through a type I photoprocess.<sup>25,26</sup>

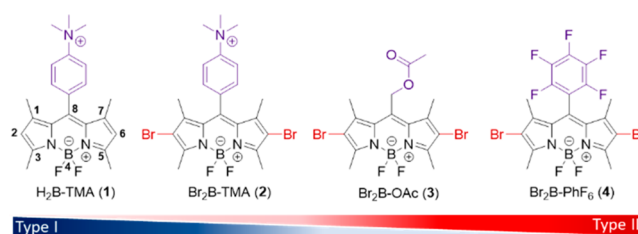


**Figure 1.** Compounds prepared and used in this work. Compounds 1 and 2 operate mainly through a type I mechanism, whereas compounds 3 and 4 involve a type II mechanism.

Subsequently, we replaced the hydrogen atoms at positions 2 and 6 in compound 1 with bromine atoms with the intention of promoting a type II photomechanism via a heavy-atom effect,<sup>27–31</sup> obtaining compound 2. Also, compounds 1 and 2 were designed to selectively bind to the cell wall by means of the cationic *N,N,N*-trimethylamino *p*-phenylene unit at the *meso* position of the BODIPY core.<sup>25</sup> On the other hand, compound 3 has a high photostability and a  $\Phi_\Delta$  value close to unity, revealing a type II photooxidation mechanism and good photoinactivating capability.<sup>32</sup> It can also form hydrogen bonds because of the presence of a *meso*-acetoxyacetyl substituent. The last PS, compound 4, was designed with a pentafluorophenyl (PFP) ring at the *meso* position of the BODIPY core, which also included heavy atoms. The presence of fluorine atoms increases cytotoxicity by binding to membrane-embedded proteins. The PFP group readily undergoes a regioselective nucleophilic replacement of the *para*-fluorine atom by a diverse set of nucleophiles.<sup>33</sup>

**Photophysical Studies.** The spectroscopic properties of BODIPYs 1–4 in acetonitrile are listed in Table 1. The main absorption band of compound 1 is centered at ~500 nm. The presence of bromine atoms at positions 2 and 6 produced a bathochromic shift of ~20 nm for compound 2 and ~40 nm for compounds 3 and 4 (Figure S1). This band was attributed to a strong  $S_0 \rightarrow S_1$  transition.<sup>34,35</sup> Furthermore, it is possible to distinguish the typical shoulder at 470 and 500 nm assigned to the 0–1 vibrational band of the same transition. Moreover, moving to the cyan zone of the spectrum, a second band at ~370 nm, attributed to the  $S_0 \rightarrow S_2$  transition, can be visualized. The fluorescence emission spectra of compounds 1–4 were also compared in acetonitrile. The bands are shown in Figure S1 and correspond to the  $S_1 \rightarrow S_0$  transition, where the presence of bromine resulted in a red-shift as a result of the resonance donating effect of the heavy atom.

All compounds evidenced a high molar extinction coefficient ( $\sim 70\text{--}80 \times 10^3 \text{ M}^{-1} \text{ cm}^{-1}$ ); in accordance with intersystem crossing taking place, compounds 3 and 4 are characterized with the lowest values of  $\Phi_f$  and the highest values for  $\Phi_\Delta$  (Table 1). However, despite having bromines and a low  $\Phi_f$ , compound 2 also has a low  $\Phi_\Delta$ , which could be attributed to aggregation of the dye in acetonitrile.<sup>36</sup> Compound 1 presented low  $^1\text{O}_2$  production, in agreement with a type I photomechanism as was previously demonstrated.<sup>25,26</sup> As will be discussed below, in the present work, by using the fluorescent reporter 2',7'-dichlorodihydrofluorescein diacetate (H<sub>2</sub>DCFDA), we elucidated that within the cellular micro-environment, both PSs proceed mainly through a type I pathway.

Finally, to compare PS efficacies, experimental conditions were optimized to adjust the number of absorbed photons during the irradiation process.

Table 1. Photophysical Properties of Compounds 1–4 in Acetonitrile at Room Temperature

compound	absorption $\lambda_{\max}$ (nm)	emission $\lambda_{\max}$ (nm)	$\epsilon \times 10^3$ ( $M^{-1} \text{ cm}^{-1}$ )	$\Phi_f$	$\Phi_{\Delta}^a$
1	502	513	85	$0.29 \pm 0.02$	$0.09 \pm 0.02$
2	524	543	70	$0.15 \pm 0.02$	$0.11 \pm 0.02$
3	543	562	$81^b$	$0.14 \pm 0.02^b$	$0.79 \pm 0.02$
4	543	561	82	$0.15 \pm 0.02$	$0.75 \pm 0.02$

<sup>a</sup>Singlet oxygen quantum yields calculated from the consumption of 9,10-dimethylanthracene using Rose Bengal as a standard.  $\Phi_{\Delta}(\text{RB}) = 0.54$ .<sup>37</sup> Errors are from triplicate experiments. <sup>b</sup>Value obtained from ref 32.

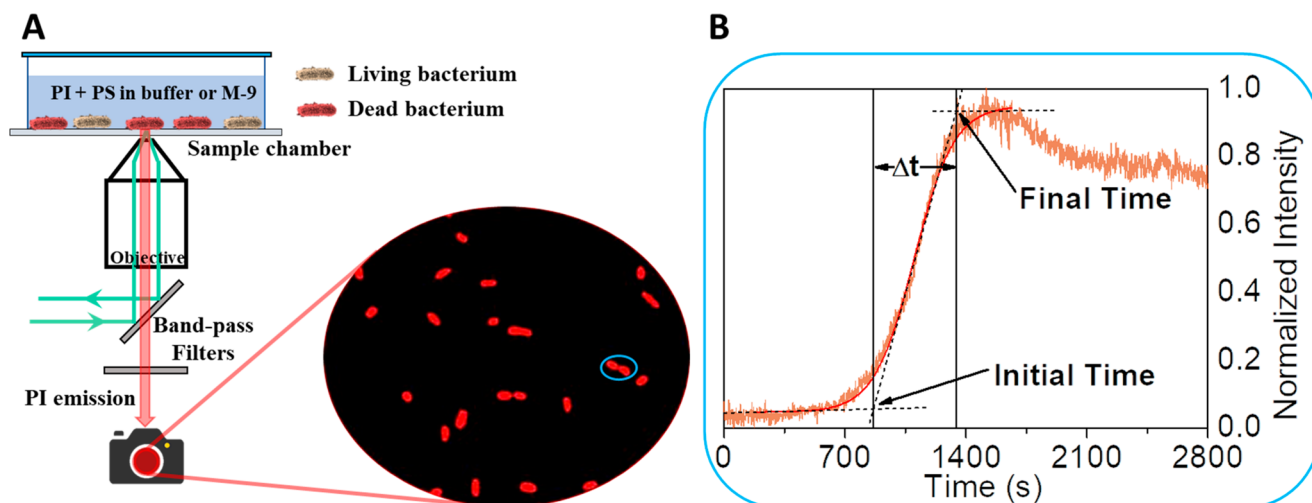


**Figure 2.** (A) Microscope setup developed for this work. After 30 min of incubation, the sample chamber was rinsed several times, leaving only bacteria attached to the glass surface. *E. coli* cells, in this case, were then exposed to  $1 \mu\text{M}$  PI to evaluate cell viability and were inactivated with  $1 \mu\text{M}$  compound 3 after 20 min of incubation in air-equilibrated PBS saline buffer (see Figure S9 for control experiments). (B) Normalized fluorescence intensity as a function of irradiation time. Fitting of the data according to eq S1 is shown by the continuous red line. The black straight lines define the initial time, the final time, and  $\Delta t = \text{final time} - \text{initial time}$ . The power of the incident light was  $0.7 \text{ J/cm}^2$ .

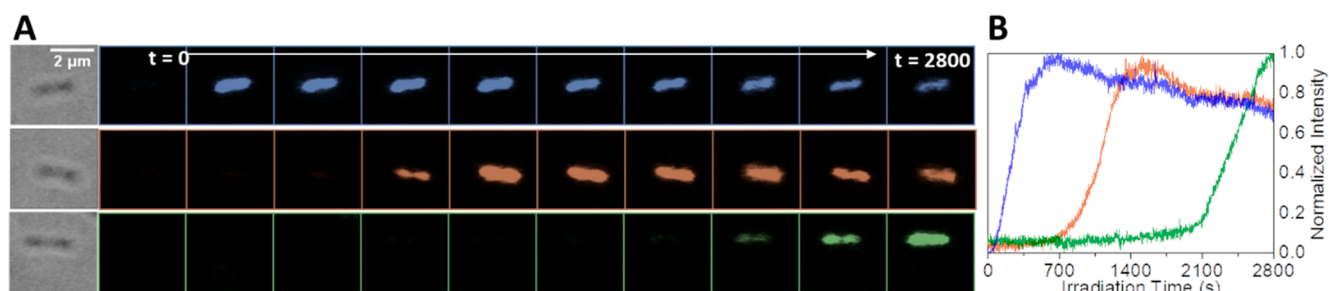


**Figure 3.** *E. coli* treated with compound 3 in the presence of PI. (A) Filmstrips corresponding to three different bacterial cells advancing (top to bottom) from more labile to more resistant. Fluorescence is due to PI incorporation. (B) Normalized fluorescence intensity as a function of irradiation time. Colored traces differentiate each bacterium in the filmstrips. Filmstrips and intensity profiles were extracted from Video S1. Control experiments are shown in the Supporting Information (Figure S9).

**PS Effectiveness at Eliminating Pathogens.** To evaluate PS efficacy and subsequently the phenotypic heterogeneity of resistance of a bacterium to the treatment, we monitored bacterial death for the four PSs in two well-studied bacterial strains: Gram-negative *E. coli* ATCC 25922 and Gram-positive methicillin-resistant *S. aureus* ATCC 43300 (MRSA). Movies with millisecond precision monitoring PI incorporation into cells were recorded until the maximum fluorescence intensity was reached for all bacteria in the imaging region. For each movie recording fluorescence from PI incorporation, a phase contrast image was acquired before and after the PDI treatment. These allowed us to carefully select only the bacteria that remained attached to the glass surface from the beginning to the end of the experiment (Figure 2A).

Bacteria that were detached from the surface, out of focus, showing fluorescence from the beginning (i.e., dead prior to treatment), or freely diffusing in solution even after careful washing of the chamber several times were not considered in the analysis. By fitting the fluorescence intensity versus time trajectories (Figure 2B) for each bacterium with a sigmoidal equation (eq S1) and by extrapolation, we defined the initial and final times. Here, the initial time refers to the time when the intensity enhancement begins; hence, we considered this the time at which the PS had elicited enough damage on the membrane so as to permit PI incorporation and DNA binding.

On the other hand, we can say that bacterial death is reached when the fluorescence enhancement reaches maximum (see Video S1), which was denoted as the final time. In addition,

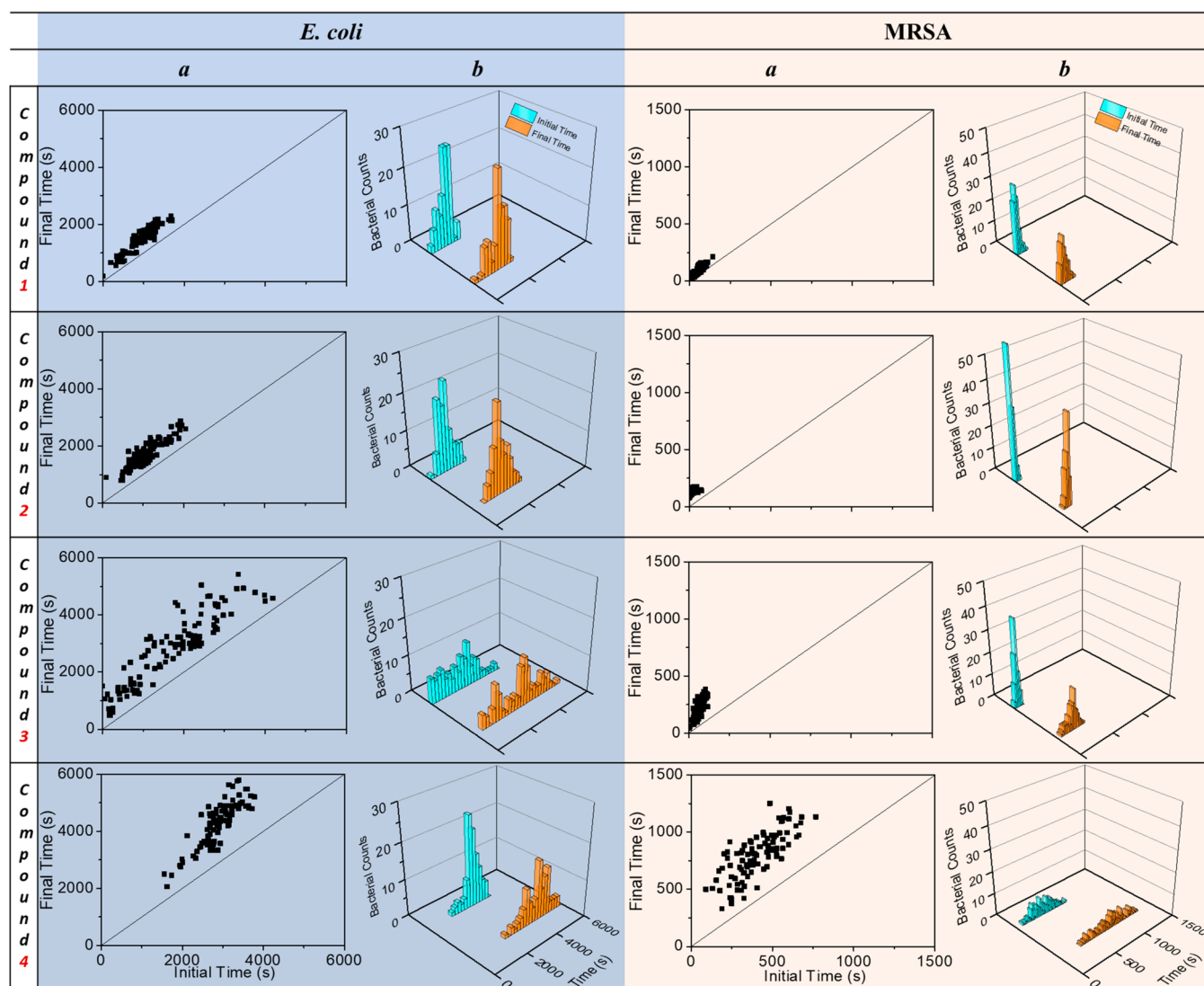


**Figure 4.** Statistical analysis for *E. coli* (light blue, left) and MRSA (light orange, right). Column *a*: scatter plots showing the correlations between the final and initial intensities. The continuous black lines were added to guide the eye and represent the cases where PI incorporates immediately ( $\Delta t = 0$ ). Column *b*: bacterial counts as functions of the initial (cyan) and final (orange) times. Rows display the compound utilized for each treatment. The light doses applied for these experiments were between 0.04 and 3.4 J/cm<sup>2</sup>.

the difference between the final and initial times ( $\Delta t$ ) was also calculated, giving insight into how long it takes PI to permeate through the cell envelope.

A total of one hundred traces for each bacterial strain coming from randomly selected bacteria were gathered and analyzed to generate plots. This approach provided statistic information about different bacterial survival times due to phenotypic differences and PS efficacy upon therapy. As it is possible to appreciate in Video S1 (100× time-lapse), every *E. coli* bacterium has a singular response to the photodamage capability of the PS (compound 3 in this case) and hence PI incorporation. This heterogeneity within the bacterial sample is better appreciated in Figure 3, which shows filmstrips and intensity profiles extracted from Video S1 at different times for three individual cells from the sample chamber. At this point, we want to remark that first, the bacterial sample came from a pure culture originating from one single isolated colony, and thus all bacteria were genetically identical, and second, to ensure that the bacteria were in the same metabolic state,

strains were cultured until they reached halfway to stationary phase.<sup>38–40</sup>

In comparison with flow cytometry (another experimental methodology commonly used for cell analysis), our experimental setting is a much simpler<sup>41</sup> technique based on fluorescence microscopy, with monitoring cells in real-time with fluorogenic probes; it is also possible to apply more than one dye with the addition of just a band-pass filter. We also point out a disadvantage: bacterial attachment to the glass surface depends on bacterial gender and the media employed.

The statistical information gathered from the movies for the experiments with *E. coli* and MRSA are assembled in Figure 4. In this figure, column *a* represents the correlation between the final and initial times, with each bacterium represented by a square in the scatter plot. These plots are also provided with a continuous black line that represents the case in which PI incorporates immediately upon PS-mediated photooxidation, meaning  $\Delta t = 0$ . As is easily appreciated in Figure 4, this is not true in our case.

Table 2. Photoinactivation Data for *E. coli* and MRSA Treated with Compounds 1–4

compound	<i>E. coli</i>							
	$\Delta t$ (s)				final time (s)			
	mean	min	max	range <sup>a</sup>	mean	min	max	range <sup>a</sup>
1	530.6	181.7	866.5	684.7	1515.1	192.2	2281.6	2089.4
2	632.9	286.5	1168.8	882.0	1717.76	800.2	2879.2	2079.1
3	1103.9	295.9	2639.8	2343.8	2820.8	491.8	5429.0	4937.2
4	1379.5	440.3	2484.8	2044.5	4241.4	2061.8	5784.5	3722.7
1 (M-9)	706.1	111.1	1967.0	1855.9	4369.2	1057.5	6779.3	5721.8
compound	MRSA							
	$\Delta t$ (s)				final time (s)			
	mean	min	max	range <sup>a</sup>	mean	min	max	range <sup>a</sup>
1	31.1	4.2	91.5	87.4	71.1	8.2	211.6	203.4
2	63.3	66.1	168.2	102	136.4	78.3	175.9	97.2
3	160.7	40.6	281.3	240.8	226.1	44.9	384.5	339.6
4	385.6	95.4	769.0	673.6	790.3	331.0	1252.6	921.6

<sup>a</sup>One-way ANOVA was applied to indicate statistical significance at  $P < 0.001$ .

Figure 4 column *b* shows 3D histograms representing the bacterial counts as functions of the initial (cyan) and final (orange) times. Rows indicate the compound that was used for each treatment. Figure 4 will be the main object of discussion in this paper.

Figure 4, particularly the scatter plots (column *a*), clearly displays that differences in bacterial inactivation times due to phenotypic heterogeneity are always present during PDI treatment but in different magnitudes. These distributions in the survival times are directly related to the PS, and that is why we will first emphasize PS efficacies in achieving membrane damage. After that, we will focus on highlighting the heterogeneity of bacterial survival due to phenotypic differences.

The variations in the initial and final times for the same bacterial strain are directly related to the PS effectiveness, for which uptake plays a crucial role. Therefore, we measured dye uptake, monitoring PS fluorescence and using an experimental approach with similar conditions to those applied during PDI experiments at the microscope (see the Material and Methods in the Supporting Information). Uptake studies for the four PSs with *E. coli* and MRSA are shown in Table S1. For *E. coli*,  $10^8$  cells incorporate 0.4 nmol of PSs 1 and 2, which is  $\sim 1.3$  and 2 times more than the levels for compounds 3 and 4, respectively. In contrast, studies in MRSA show that compounds 3 and 4 exhibit uptake values 2 times higher than those of compounds 1 (0.3 nmol for  $10^8$  cells) and 2 (0.4 nmol for  $10^8$  cells). Moreover, similar binding was found for cationic PSs 1 and 2 in both bacteria, whereas considerable increases were obtained for 3 and 4 in *S. aureus* cells with respect to those in *E. coli* cells.

The results can be explained by looking at the differences in the compositions of the outer envelopes between the Gram-negative and Gram-positive models. Specifically, the cell wall of Gram-positive bacteria are formed by two layers, a lipid bilayer and a thick peptidoglycan layer (30–100 nm) containing teichoic acid.<sup>42</sup> Overall, this barrier has a negative net charge and is permeable because it is relatively porous.<sup>43</sup> In contrast, in Gram-negative bacteria, the cytoplasm is protected by an inner lipid membrane and a highly complex multilayered structure constituted by a compacted peptidoglycan film (2–10 nm) to which the outer membrane is attached.<sup>44</sup> The outer membrane presents an asymmetric lipid structure formed by

negatively charged lipopolysaccharides (LPS), lipoproteins, and proteins with porin functions. Molecules of LPS yield a polyanionic external surface, which is partially neutralized by the divalent cations  $Mg^{2+}$  and  $Ca^{2+}$ .<sup>43,45,46</sup> Thus, compounds 1 and 2, bearing cationic groups, can penetrate deeper into the outer membrane of *E. coli* and produce tight electrostatic interactions with negatively charged sites. This effect can increase the photocytotoxicity mediated by the PSs. In contrast, compounds 3 and 4 can bind through either hydrogen bonds or covalent interactions with the peripheral polysaccharide groups on the LPS chains. In consequence, besides the higher binding values, ROS are more cytotoxic when they are produced by compounds 1 and 2 because they are located in close proximity to lipids and membrane-embedded proteins. This is not the case with compounds 3 and 4, which produce  $^1O_2$  on the periphery. As aforementioned, Gram-positive bacteria have a thicker and porous peptidoglycan layer that can uptake better compounds 3 and 4. In fact, PS 3, because of its reduced size, can probably penetrate deeper into the outer membrane, producing major damage. Nevertheless, the amphiphilic characters of compounds 1 and 2 not only increase their solubility in biological environments but also enhance binding and penetration into microbial cells.<sup>47</sup>

As expected by the cell wall composition, the PSs inactivated MRSA in less time than they did *E. coli*. Specifically, compounds 1, 2, 3, and 4 annihilated MRSA 11, 16, 14, and 5 times faster than they did *E. coli* (Table 2, final times, maximum values). This is also visualized well in the supporting videos (Videos S2 and S3, 100 $\times$  time-lapse), which show *E. coli* and MRSA inactivation with compound 1. Another factor to be considered here is the mechanism by which the PS generates the photodynamic action. ROS produced through a type I mechanism are longer living than  $^1O_2$ , and hence they can diffuse longer and attack a larger number of biomolecules.<sup>7</sup> In particular, Hamblin and co-workers hypothesized that PSs operating through a type I mechanism are better at killing Gram-negative bacteria than those operating through a type II mechanism. They proposed that  $^1O_2$  could diffuse better into the porous cell walls of Gram-positive bacteria, whereas the less permeable Gram-negative bacterial outer envelope needs the more reactive radicals to cause real damage.<sup>48,49</sup> In order to predict and visualize the radical pathway that takes place within

the cells, we performed assays using the same experimental approach but with prior incubation with the ROS fluorogenic quencher  $H_2DCFDA$ .<sup>50</sup>

The results show that the probe reached a maximum intensity in only 200 s when *E. coli* was treated with compound 1 (see Figure S19). On the other hand, no fluorescence enhancement was observed when compound 3 was used for the therapy. Interestingly, inactivation with compound 2 also showed fluorescence after 550 s of irradiation. This assay revealed that the mechanisms taking place within the bacterial environment are mainly type I for compounds 1 and 2.

We mentioned above higher phenotypic resistance to PDI therapy, which we attributed to differences in the bacterial wall. However, another possibility is that the phenotypic variation affects the uptake of the PS, resulting in differential membrane damage by ROS and variations in PI permeation. To evaluate this second possibility, uptake assays of compound 3 in *E. coli* were also performed at the single bacterium level but without PI. All bacteria reached the same fluorescence intensity in less than 5 min, indicating that phenotypic differences did not affect PS uptake (Video S4). A third factor that could be mediating the differences in cell killing is the intrinsic bacterial defense systems (enzymatic and nonenzymatic).<sup>51</sup> The most well-characterized and studied bacterial model is *E. coli*, where scavenging systems are enough to protect the cell under an aerobic environment.<sup>52,53</sup> Although hazardous exogenous sources, such as PDI, elevate the rates of ROS triggering in the cell, it was observed that under such conditions, the levels of the bacterial defenses become insufficient.<sup>53</sup>

Given the success of compound 1, we subsequently tested its PDI capabilities in two other Gram-negative strains, a reference *Pseudomonas aeruginosa* strain (ATCC 27853) and a clinical strain of *Klebsiella pneumoniae*. Together with *E. coli* and MRSA, we selected these four strains, all ESKAPE pathogens, because of the elevated numbers of nosocomial infections reported in the last few years and because of their ability to present MDR phenotypes. In February 2017, the World Health Organization launched a list of antibiotic-resistant priority pathogens for which we are in imminent need of the development of new drugs or therapies to battle against them;<sup>54</sup> our strains are included on the list. A full representation of the results obtained with compound 1 and all the Gram-negative bacteria treated here are represented in Figure S3. In this figure, as well as in all the figures showing statistical data in this work, analysis for each bacterial strain is represented by a colored pattern. The results point out that the three pathogens exhibit similar responses to the treatment. Overall, the three strains had low dispersity time values for both the correlation plots and the histograms, with final times below 2000 s (Table S2).

**Bacterial Phenotypic Heterogeneity.** As seen in Figure 4, column *a*, the scatter plots indicate that the major population heterogeneity in *E. coli* was observed with compound 3. The population dispersion rates ranged from ~500 to 5500 s, accounting for a gap of ~5000 s between the first and the last inactivated bacteria (Table 2, final times, range). This effect is better visualized in column *b*, where the histograms show 52% overlaps between the initial and final incorporation times and large dispersion of bacterial death times. The same bacterial heterogeneity was observed in *P. aeruginosa* treated with compound 3 (Figure S4). On the other hand, we found localized trends with less heterogeneity and smaller time windows when compounds 1 and 2 were

employed as the PSs (Figure 4, first and second rows). In these experiments, histogram overlapping was ~35% in both cases, and the final times for complete PI incorporation went from 200 to 2200 s for compound 1 and from 800 to 2900 s for compound 2 (Table 2). On average, these two PSs killed ~2 times faster than compound 3. Treatment with compound 4 also exhibited a localized bacterial population, with a gap time 1.8 times larger than those of compounds 1 and 2 and 1.3 times smaller than that of compound 3 (Table 2, final time, mean values). Although compound 4 has less dispersity than PS 3, it presents the longest survival times.

Conversely, the widest population distribution and the longest death times in MRSA were observed when the Gram-positive bacteria were treated with compound 4 (Figure 4 and Table 2). In this case, the difference between the initial and final times was 4.5, 9.5, and 1.7 times bigger than those for compounds 1, 2, and 3, respectively (Table 2). For this strain, Compound 2 showed the lowest bacterial phenotypic heterogeneity (Figure 4, MRSA, column *b*), and the difference between the first and the last inactivated bacterium was only 97 s (Table 2, final times, range). Compound 4 presented intermediate dispersity in the scatter plot and the largest full width half maximum for the Gaussian shape.

**Membrane Damage and PI Incorporation Times.** As described above, squares that represent a unique bacterial behavior clearly deviate from a slope of 1 (continuous black line) in the scatter plots in Figure 4, indicating that there is a specific PI incorporation period for each bacterium. This lag time is further evidence of phenotypic differences expressed in cell wall composition. To extend the analysis further, we studied the correlation between  $\Delta t$  (defined in Figure 2) and the final time results that are shown in Figure S5. Figure S5 is composed of scatter plots; the columns depict the PS used for the inactivation, and the rows correspond to the bacterial strain and are highlighted with specific colors. As can be appreciated in all the plots, bacteria with short survival times have small PI incorporation periods, whereas the opposite takes place for bacteria with long inactivation times. This is better observed in the inset of Figure S5, where the normalized intensity versus final time profile is represented for two bacteria with different phenotypes but from the same population under therapy. For instance, a bacterium with a survival time (black trace) of 1080 s has  $\Delta t = 340$  s, and a bacterium with a survival time of 3240 s (orange trace) has  $\Delta t = 1036$  s. These tendencies are linearly related by eq S2. Furthermore, the plots in Figure S5 also indicate that there is a singular slope to be applied in eq S2 for every experimental condition (e.g., for *E. coli* treated with compound 1, the slope is 2.47, and for MRSA treated with compound 3, the slope is 1.21). In general, correlations for each bacterial strain provided values between ~1 and 3, depending on the PS used. Accordingly, with eq S2, the death time for an *E. coli* bacterium treated with PS 1 is going to be given by 2.47 multiplied by the incorporation time (final time =  $2.47 \times \Delta t$ ). Of course, incorporation times also vary according to bacterial strain and the potential of the PS to achieve membrane damage. This experimental evidence certainly demonstrates that within the same therapeutic conditions, a bacterium with higher phenotypic resistance can endure the treatment for longer periods. Thus, membrane damage seems to be less severe allowing slower PI incorporation compared with that in vulnerable individuals.

Comparing bacterial strains as a consequence of the cell wall composition (discussed above, mean values in Table 2 under

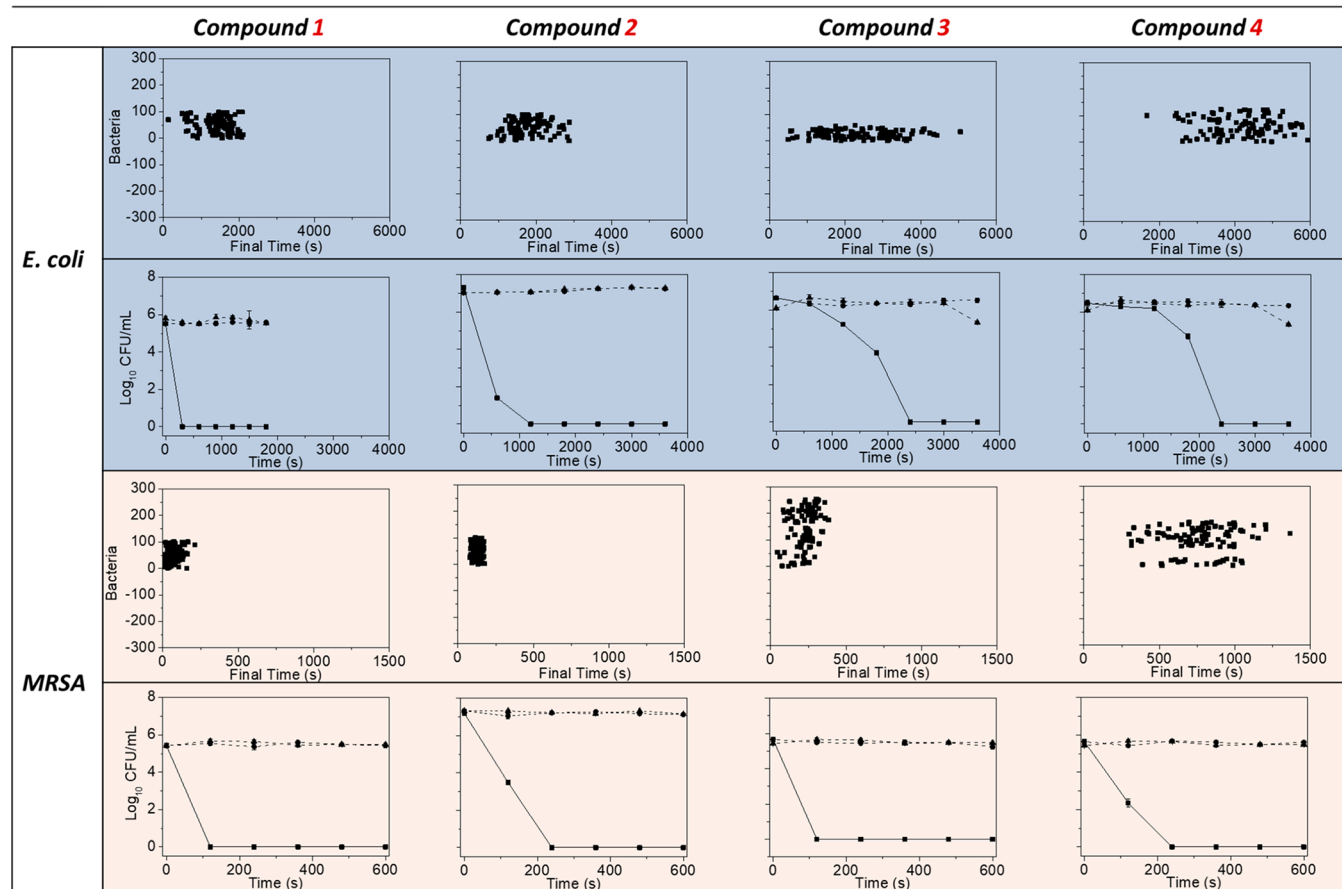


**Figure 5.** Correlation between bacteria and final times (top rows) and time–kill curves (bottom rows) for *E. coli* (light blue) and MRSA (light red). Columns represent the PS used in the treatment. Time–kill curve profiles are shown with the following encoding symbols: bacteria and light (basal condition), ●; bacteria and PS in the dark (PS control), ▲; bacteria with PS and light (PDI treatment), ■. Results represent means  $\pm$  standard deviations (SD) from three independent experiments. The light doses employed to eliminate the bacterial populations in the time–kill curve experiments for *E. coli* were 1.5, 3, 12, and 12 J/cm<sup>2</sup> for compounds 1, 2, 3, and 4, respectively, whereas MRSA needed 0.6, 1.2, 0.6, and 1.2 J/cm<sup>2</sup> doses for compounds 1, 2, 3, and 4, respectively.

$\Delta t$ ) indicates that incorporation times are on average 17, 10, 7, and 4 times faster for MRSA than for *E. coli*, advancing from compound 1 to 4. Moreover, the binding and photooxidative effectiveness of the PSs are also reflected in PI incorporation times. As can be appreciated in Table 2, for both bacterial strains, compounds 1 and 2 have the shortest incorporation periods in all cases, followed by compounds 3 and 4.

**Bacterial PDI under Cell Growth Conditions.** The advantages of this imaging technique are not only simplicity and real-time cell death monitoring. It also permitted us to monitor cells in growth conditions and in a potential first stage of biofilm formation, in which a bacterium finds a substrate and attaches to it in a reversible form that becomes an irreversible state.<sup>55,56</sup> This system allows cells to start signaling to continue biofilm aggregation. Biofilms are the principal cause of antibiotic treatment failure because of their ability to protect cells inside the matrix from environmental threats.<sup>57</sup>

As a step forward, we provided bacteria with adequate medium to grow. Minimal medium (M-9) was used as the working solution instead of regular PBS saline buffer. These results are shown in the last row of Figure S3 (*E. coli* + M-9) and are converted to the numbers shown in Table 2 (*E. coli* + M-9). We chose compound 1 for this experiment because of its efficacy. After treatment with compound 1, *E. coli* population death time heterogeneity and bacterial survival times increased

significantly with this source of energy, although PS binding was similar (see Table S1). The final time ranges and mean values were  $\sim 3$  times longer than those for *E. coli* in PBS saline buffer. Moreover, the PI incorporation time also increased by a factor of 1.3. These data manifest how bacteria are less vulnerable to therapy in growth conditions and how they can behave in real scenarios.

**Time–Kill Curve Profiles in PDI.** Time–kill curve profiles allow the classification of antibiotics as bactericidal or bacteriostatic compounds when the specific molecular target is unknown.<sup>58</sup> Likewise, the different antibiotic targets indicate the bacterial responses to the treatment, and these curves can be used to assess useful antibiotic combination for facing MDR bacteria in hospitals.<sup>59</sup> Also, these curves are applied to estimate regrowth of *in vitro* and *in vivo* models.<sup>60</sup> However, the curves do not give insights into single bacterium phenotypic behavior in response to the antibiotic therapy. Starting out from this premise, we focused our endeavor on demonstrating the existence of vulnerable and more resistant subpopulations in PDI and on describing, at the single bacterium level, the outline of the time–kill curve. Up to now, according to our knowledge, there is not strong experimental evidence in the literature that supports this theory, particularly in the PDI field. We believed that our experimental technique could provide further contributions in this regard. Sub-

sequently, we compared our microscopically acquired experimental data with time–kill curves. To simulate the conditions used in our experiments at the single bacterium level, we kept a genetically identical population by inoculating a single colony from a pure culture. After incubation at 37 °C for 16 h and dilution to 10<sup>6</sup> CFU/mL, we proceeded with a conventional inactivation experiment that involved the plotting of time–kill curves.

These data are represented in Figure 5, which shows the single bacterium data analysis and the time–kill curves for *E. coli* (light blue rows) and MRSA (light orange rows). Also, the PSs used for each treatment are specified on each column. As can be appreciated in this figure, both phenotypic heterogeneity and PS effectiveness show surprisingly accurate matching results for both individual bacteria and planktonic bulk experiments. As previously mentioned, compounds 1 and 2 were the most efficient PSs, inactivating both Gram-positive and Gram-negative bacteria. This tendency continued in the time–kill curves, in which the log<sub>10</sub> CFU versus time profiles for compounds 1 and 2 presented the steepest slopes for *E. coli*, followed by those for compounds 4 and 3. The largest range of phenotypic heterogeneity treatment resistance for compound 3 is reflected in the softest slope. Thus, photoinactivation slowly decreases with the initial death of the more labile population at short time intervals, which is followed by the death of more resistant microbes at longer times. Time–kill profiles for the inactivation of MRSA (Figure 5) indicate fast inactivation times and small phenotypic treatment resistance for compounds 1 and 2, evidenced by an abrupt slope and short killing time results that correlated with the single bacterium experiments. Also, in correlation with the previous experiments in this manuscript, the inactivation plot in planktonic culture for compound 4 has a smoother slope, highlighting phenotypic heterogeneity. Overall, phenotypic heterogeneity and PS efficiency once again prevailed in determining killing curve profiles.

Finally, the correlation between our single bacterium experiments and the time–kill curve assays was corroborated for *E. coli* with compound 1 in M-9 minimal medium (Figure S6). Under these conditions, the time–kill profiles showed increases in bacterial survival times and a smoother slope, indicating wider phenotypic heterogeneity in the presence of the minimal medium as compared with in PBS saline buffer.

## CONCLUSION

The simple experimental setup used in this work allowed us to characterize PDI in real-time at the single bacterium level. The methodology used is mainly based on the capability of a bacterium to attach to the glass surface, which is directly related to bacterial growth conditions and pilus formation. The experimental setup offers a clean alternative with no additional additives (e.g., polyethylenimine or agarose pads) between bacteria and surface, avoiding possible dye interactions with the glass and hence lowering background fluorescence. Furthermore, the methodology applied herein also permitted us to evaluate PS efficacy, showing that compounds 1 and 2 were outstandingly effective at inactivating Gram-positive and Gram-negative bacteria, including ESKAPE members. This is a point that should be distinguished, because not all PSs have this versatility in killing pathogens, even when cells are treated in optimal conditions such as M-9 minimal medium. In addition, the results gathered for individual bacteria provided

direct and unique experimental evidence that supports the time–kill curve profiles.

Fluorescence microscopy of an individual cell with spatiotemporal resolution gives us insight into how a bacterium can resist PDI treatment according to its distinct phenotype. Interestingly, no survivors were observed after the irradiation time selected for each experiment, demonstrating at the single bacterium level that PDI is a valuable platform for eliminating pathogens. Like any other individual of any other species on earth, each bacterium presents unique phenotypic characteristics and behavior that should be considered to achieve successful PDI treatments.

## EXPERIMENTAL SECTION

**Materials.** All chemicals were purchased from Sigma-Aldrich (Milwaukee, WI) and used without further purification. Tryptic soy broth and agar were purchased from Britania (Buenos Aires, Argentina).

**Instrumentation.** UV–visible absorption spectra were acquired on a Shimadzu UV-2401PC spectrometer (Shimadzu Corporation, Tokyo, Japan). Luminescence spectra were recorded using a Spex FluoroMax spectrofluorometer (Horiba Jobin Yvon Inc., Edison, NJ). Fluence rates were obtained with a Radiometer Laser Mate-Q (Coherent, Santa Clara, CA). Photooxidation of DMA and bacterial photoinactivation in planktonic media were performed using a light-emitting diode (LED) array that emitted green light at a center wavelength of 510 nm with a fluence rate of 5 mW/cm<sup>2</sup>. Proton nuclear magnetic resonance spectra were acquired on a Bruker Avance 300 FT-NMR spectrometer. Mass spectra were measured on a Bruker micro-TOF-QII spectrometer (Bruker Daltonics, MA) equipped with an ESI source (ESI-MS). Silica gel thin-layer chromatography (TLC) plates (250 mm) were acquired from Analtech (Newark, DE). Silica gel 60 (0.040–0.063 mm, 230–400 mesh) from Merck (Darmstadt, Germany) was used for flash column chromatography. Microscopic observations were made with an inverted fluorescence microscope (BIM500FL, Bioimager, ON, Canada).

## ASSOCIATED CONTENT

### Supporting Information

The Supporting Information is available free of charge on the ACS Publications website at DOI: 10.1021/acsinfecdis.9b00185.

Steady-state fluorescence studies, fluorescence quantum yields, determination of <sup>1</sup>O<sub>2</sub> quantum yield (photooxidation of DMA, indirect method), strains and culture conditions, uptake studies, imaging assays, image processing, assays with H<sub>2</sub>DCFDA, biological assays (antibacterial photodynamic inactivation studies in *E. coli* ATCC 25922 and MRSA), control experiments, synthetic procedures, and characterization of compounds 2 and 4 (PDF)

Video S1 (AVI)

Video S2 (AVI)

Video S3 (AVI)

Video S4 (AVI)

## AUTHOR INFORMATION

### Corresponding Author

\*E-mail: adurantini@exa.unrc.edu.ar.

ORCID 

Andrés M. Durantini: 0000-0002-7898-4033

## Notes

The authors declare no competing financial interest.

## ACKNOWLEDGMENTS

S.R.M., D.A.H., M.L.A., and A.M.D are grateful to Consejo Nacional de Investigaciones Científicas y Técnicas (CONICET) of Argentina. Y.B.P. is grateful to the Agencia Nacional de Promoción Científica y Tecnológica (ANPCYT). S.R.M. and A.M.D. are thankful to their daughter Bianca for bringing so much joy to their lives. We appreciate the financial support from the Agencia Nacional de Promoción Científica y Tecnológica (FONCyT), Argentina.

## REFERENCES

- (1) Blair, J. M. A., Webber, M. A., Baylay, A. J., Ogbolu, D. O., and Piddock, L. J. V. (2015) Molecular mechanisms of antibiotic resistance. *Nat. Rev. Microbiol.* 13, 42.
- (2) Knopp, M., and Andersson, D. I. (2018) Predictable Phenotypes of Antibiotic Resistance Mutations. *mBio* 9 (3), No. e00770-18.
- (3) Ventola, C. L. (2015) The antibiotic resistance crisis: part 1: causes and threats. *Pharm. Ther.* 40 (4), 277–283.
- (4) Zhang, Q., Lambert, G., Liao, D., Kim, H., Robin, K., Tung, C.-k., Pourmand, N., and Austin, R. H. (2011) Acceleration of Emergence of Bacterial Antibiotic Resistance in Connected Micro-environments. *Science (Washington, DC, U. S.)* 333 (6050), 1764–1767.
- (5) Burki, T. K. (2018) Superbugs: An Arms Race Against Bacteria. *Lancet Respir. Med.* 6 (9), 668.
- (6) Turro, N. J., Ramamurthy, V., and Scaiano, J. C. (2012) *Modern Molecular Photochemistry of Organic Molecules*, University Science Books.
- (7) Ogilby, P. R. (2010) Singlet oxygen: there is indeed something new under the sun. *Chem. Soc. Rev.* 39 (8), 3181–209.
- (8) Schweitzer, C., and Schmidt, R. (2003) Physical mechanisms of generation and deactivation of singlet oxygen. *Chem. Rev.* 103 (5), 1685–757.
- (9) Ziegelhoffer, E. C., and Donohue, T. J. (2009) Bacterial responses to photo-oxidative stress. *Nat. Rev. Microbiol.* 7 (12), 856–63.
- (10) Finkel, T., and Holbrook, N. J. (2000) Oxidants, oxidative stress and the biology of ageing. *Nature* 408, 239.
- (11) Phaniendra, A., Jestadi, D. B., and Periyasamy, L. (2015) Free radicals: properties, sources, targets, and their implication in various diseases. *Indian J. Clin. Biochem.* 30 (1), 11–26.
- (12) Nishikawa, T., Edelstein, D., Du, X. L., Yamagishi, S.-i., Matsumura, T., Kaneda, Y., Yorek, M. A., Beebe, D., Oates, P. J., Hammes, H.-P., Giardino, I., and Brownlee, M. (2000) Normalizing mitochondrial superoxide production blocks three pathways of hyperglycaemic damage. *Nature* 404, 787.
- (13) Nemoto, S., Takeda, K., Yu, Z. X., Ferrans, V. J., and Finkel, T. (2000) Role for mitochondrial oxidants as regulators of cellular metabolism. *Mol. Cell. Biol.* 20 (19), 7311–7318.
- (14) Brauner, A., Fridman, O., Gefen, O., and Balaban, N. Q. (2016) Distinguishing between resistance, tolerance and persistence to antibiotic treatment. *Nat. Rev. Microbiol.* 14, 320.
- (15) Davies, J., and Davies, D. (2010) Origins and evolution of antibiotic resistance. *Microbiology and molecular biology reviews: MMBR* 74 (3), 417–33.
- (16) Balaban, N. Q., Merrin, J., Chait, R., Kowalik, L., and Leibler, S. (2004) Bacterial Persistence as a Phenotypic Switch. *Science (Washington, DC, U. S.)* 305 (5690), 1622–1625.
- (17) Kussell, E. L., Kishony, R., Balaban, N. Q., and Leibler, S. (2005) Bacterial persistence: a model of survival in changing environments. *Genetics* 169, 1807.
- (18) Lewis, K. (2007) Persistor cells, dormancy and infectious disease. *Nat. Rev. Microbiol.* 5, 48.
- (19) Pulzova, L., Navratilova, L., and Comor, L. (2017) Alterations in Outer Membrane Permeability Favor Drug-Resistant Phenotype of *Klebsiella pneumoniae*. *Microb. Drug Resist.* 23 (4), 413–420.
- (20) Soto, S. M. (2013) Role of efflux pumps in the antibiotic resistance of bacteria embedded in a biofilm. *Virulence* 4 (3), 223–229.
- (21) Williams, S., Hong, Y., Danavall, D., Howard-Jones, M., Gibson, D., Frischer, M., and Verity, P. (1998) Distinguishing between living and nonliving bacteria: evaluation of the vital stain propidium iodide and its combined use with molecular probes in aquatic samples. *J. Microbiol. Methods* 32 (3), 225–236.
- (22) Kramer, C. E., Wiechert, W., and Kohlheyer, D. (2016) Time-resolved, single-cell analysis of induced and programmed cell death by non-invasive propidium iodide and counterstain perfusion. *Sci. Rep.* 6, 32104.
- (23) Johnson, M. B., and Criss, A. K. (2013) Fluorescence microscopy methods for determining the viability of bacteria in association with mammalian cells. *J. Visualized Exp.* No. 79, e50729.
- (24) Boucher, H. W., Talbot, G. H., Bradley, J. S., Edwards, J. E., Gilbert, D., Rice, L. B., Scheld, M., Spellberg, B., and Bartlett, J. (2009) Bad bugs, no drugs: no ESCAPE! An update from the Infectious Diseases Society of America. *Clin. Infect. Dis.* 48 (1), 1–12.
- (25) Agazzi, M. L., Ballatore, M. B., Reynoso, E., Quiroga, E. D., and Durantini, E. N. (2017) Synthesis, spectroscopic properties and photodynamic activity of two cationic BODIPY derivatives with application in the photoinactivation of microorganisms. *Eur. J. Med. Chem.* 126, 110–121.
- (26) Reynoso, E., Quiroga, E. D., Agazzi, M. L., Ballatore, M. B., Bertolotti, S. G., and Durantini, E. N. (2017) Photodynamic inactivation of microorganisms sensitized by cationic BODIPY derivatives potentiated by potassium iodide. *Photochem. Photobiol. Sci.* 16 (10), 1524–1536.
- (27) Kamkaew, A., Lim, S. H., Lee, H. B., Kiew, L. V., Chung, L. Y., and Burgess, K. (2013) *Chem. Soc. Rev.* 42 (1), 77–88.
- (28) Yogo, T., Urano, Y., Ishitsuka, Y., Maniwa, F., and Nagano, T. (2005) Highly efficient and photostable photosensitizer based on BODIPY chromophore. *J. Am. Chem. Soc.* 127 (35), 12162–3.
- (29) Lu, Z. T., Zhang, X. G., Wu, Z. M., Zhai, T. T., Xue, Y. A., Mei, L., and Li, C. X. (2014) BODIPY-based macromolecular photosensitizer with selective recognition and enhanced anticancer efficiency. *RSC Adv.* 4 (37), 19495–19501.
- (30) Ma, J., Yuan, X. L., Kucukoz, B., Li, S. F., Zhang, C. S., Majumdar, P., Karatay, A., Li, X. H., Yaglioglu, H. G., Elmali, A., Zhao, J. Z., and Hayvali, M. (2014) Resonance energy transfer-enhanced rhodamine-styryl Bodipy dyad triplet photosensitizers. *J. Mater. Chem. C* 2 (20), 3900–3913.
- (31) Guo, S., Ma, L. H., Zhao, J. Z., Kucukoz, B., Karatay, A., Hayvali, M., Yaglioglu, H. G., and Elmali, A. (2014) BODIPY triads triplet photosensitizers enhanced with intramolecular resonance energy transfer (RET): broadband visible light absorption and application in photooxidation. *Chem. Sci.* 5 (2), 489–500.
- (32) Durantini, A. M., Greene, L. E., Lincoln, R., Martínez, S. R., and Cosa, G. (2016) Reactive Oxygen Species Mediated Activation of a Dormant Singlet Oxygen Photosensitizer: From Autocatalytic Singlet Oxygen Amplification to Chemically Controlled Photodynamic Therapy. *J. Am. Chem. Soc.* 138 (4), 1215–1225.
- (33) Gutsche, C. S., Ortwerth, M., Gräfe, S., Flanagan, K. J., Senge, M. O., Reissig, H.-U., Kulak, N., and Wiehe, A. (2016) Nucleophilic Aromatic Substitution on Pentafluorophenyl-Substituted Dipyrranes and Tetrapyrroles as a Route to Multifunctionalized Chromophores for Potential Application in Photodynamic Therapy. *Chem. - Eur. J.* 22 (39), 13953–13964.
- (34) Baruah, M., Qin, W., Flors, C., Hofkens, J., Vallée, R. A. L., Beljonne, D., Van der Auweraer, M., De Borggraeve, W. M., and Boens, N. (2006) Solvent and pH Dependent Fluorescent Properties of a Dimethylaminostyryl Borondipyromethene Dye in Solution. *J. Phys. Chem. A* 110 (18), 5998–6009.

- (35) Shivran, N., Tyagi, M., Mula, S., Gupta, P., Saha, B., Patro, B. S., and Chattopadhyay, S. (2016) Syntheses and photodynamic activity of some glucose-conjugated BODIPY dyes. *Eur. J. Med. Chem.* *122*, 352–365.
- (36) Caruso, E., Banfi, S., Barbieri, P., Leva, B., and Orlandi, V. (2012) Synthesis and antibacterial activity of novel cationic BODIPY photosensitizers. *J. Photochem. Photobiol., B* *114*, 44–51.
- (37) Wilkinson, F., Helman, W. P., and Ross, A. B. (1993) Quantum Yields for the Photosensitized Formation of the Lowest Electronically Excited Singlet State of Molecular Oxygen in Solution. *J. Phys. Chem. Ref. Data* *22* (1), 113–262.
- (38) Pepper, I. L., Gerba, C. P., Gentry, T. J., and Maier, R. M. (2011) *Environmental microbiology*, Academic Press.
- (39) Paulton, R. J. L. (1991) The bacterial growth curve. *J. Biol. Educ.* *25* (2), 92–94.
- (40) Gefen, O., Fridman, O., Ronin, I., and Balaban, N. Q. (2014) Direct observation of single stationary-phase bacteria reveals a surprisingly long period of constant protein production activity. *Proc. Natl. Acad. Sci. U. S. A.* *111* (1), 556–561.
- (41) Flow cytometry is a powerful tool for counting, detecting, and separating subpopulations of cells. Also, it is used to identify changes in cellular function and metabolic activity and has recently been used to recognize expressed genes. However, in order to achieve appropriate results, a combination of diverse dyes is crucial, and to improve data collection, drawing upon other specific methodologies is needed; for instance, to investigate molecular mechanisms, the use of transcriptomic or proteomic signatures is required. Overall, flow cytometry is not a simple technique; it requires expensive equipment and qualified personal to acquire and interpret the results. In addition, in order to minimize false positive signals and artifacts, it is very important to have rigorous characterization of the dye sensitivity and specificity.
- (42) Rajagopal, M., and Walker, S. (2015) in *Protein and Sugar Export and Assembly in Gram-positive Bacteria*, pp 1–44, Springer.
- (43) Ruiz, N., Kahne, D., and Silhavy, T. J. (2006) Advances in understanding bacterial outer-membrane biogenesis. *Nat. Rev. Microbiol.* *4*, 57.
- (44) Huang, K. C., Mukhopadhyay, R., Wen, B., Gitai, Z., and Wingreen, N. S. (2008) Cell shape and cell-wall organization in Gram-negative bacteria. *Proc. Natl. Acad. Sci. U. S. A.* *105* (49), 19282–19287.
- (45) Dai, T., Huang, Y.-Y., and Hamblin, M. R. (2009) Photodynamic therapy for localized infections—State of the art. *Photodiagn. Photodyn. Ther.* *6* (3), 170–188.
- (46) Lambrechts, S. A., Aalders, M. C., Langeveld-Klerks, D. H., Khayali, Y., and Lagerberg, J. W. (2004) Effect of monovalent and divalent cations on the photoinactivation of bacteria with meso-substituted cationic porphyrins. *Photochem. Photobiol.* *79* (3), 297–302.
- (47) Durantini, A. M., Heredia, D. A., Durantini, J. E., and Durantini, E. N. (2018) BODIPYs to the rescue: Potential applications in photodynamic inactivation. *Eur. J. Med. Chem.* *144*, 651–661.
- (48) Huang, Y.-Y., Sharma, S. K., Yin, R., Agrawal, T., Chiang, L. Y., and Hamblin, M. R. (2014) Functionalized fullerenes in photodynamic therapy. *J. Biomed. Nanotechnol.* *10* (9), 1918–1936.
- (49) Huang, L., Xuan, Y., Koide, Y., Zhiyentayev, T., Tanaka, M., and Hamblin, M. R. (2012) Type I and Type II mechanisms of antimicrobial photodynamic therapy: an in vitro study on gram-negative and gram-positive bacteria. *Lasers Surg. Med.* *44* (6), 490–499.
- (50) Chen, X., Zhong, Z., Xu, Z., Chen, L., and Wang, Y. (2010) 2',7'-Dichlorodihydrofluorescein as a fluorescent probe for reactive oxygen species measurement: Forty years of application and controversy. *Free Radical Res.* *44* (6), 587–604.
- (51) Kohanski, M. A., Dwyer, D. J., and Collins, J. J. (2010) How antibiotics kill bacteria: from targets to networks. *Nat. Rev. Microbiol.* *8*, 423.
- (52) Mishra, S., and Imlay, J. (2012) Why do bacteria use so many enzymes to scavenge hydrogen peroxide? *Arch. Biochem. Biophys.* *525* (2), 145–160.
- (53) Imlay, J. A. (2013) The molecular mechanisms and physiological consequences of oxidative stress: lessons from a model bacterium. *Nat. Rev. Microbiol.* *11* (7), 443–54.
- (54) (2017) WHO publishes list of bacteria for which new antibiotics are urgently needed, *World Health Organization*, <https://www.who.int/news-room/detail/27-02-2017-who-publishes-list-of-bacteria-for-which-new-antibiotics-are-urgently-needed> (accessed July 2019).
- (55) Lambert, G., Bergman, A., Zhang, Q., Bortz, D., and Austin, R. (2014) Physics of biofilms: the initial stages of biofilm formation and dynamics. *New J. Phys.* *16* (4), 045005.
- (56) Koo, H., Allan, R. N., Howlin, R. P., Stoodley, P., and Hall-Stoodley, L. (2017) Targeting microbial biofilms: current and prospective therapeutic strategies. *Nat. Rev. Microbiol.* *15*, 740.
- (57) Donlan, R. M. (2001) Biofilm Formation: A Clinically Relevant Microbiological Process. *Clin. Infect. Dis.* *33* (8), 1387–1392.
- (58) Scholar, E. M., and Pratt, W. B., Eds. (2000) *The antimicrobial drugs*, Oxford University Press.
- (59) Bartosz, G. (2006) Use of spectroscopic probes for detection of reactive oxygen species. *Clin. Chim. Acta* *368* (1–2), 53–76.
- (60) Firsov, A. A., Vostrov, S. N., Shevchenko, A. A., and Cornaglia, G. (1997) Parameters of bacterial killing and regrowth kinetics and antimicrobial effect examined in terms of area under the concentration-time curve relationships: action of ciprofloxacin against *Escherichia coli* in an in vitro dynamic model. *Antimicrob. Agents Chemother.* *41* (6), 1281–1287.